Int. J. Electrochem. Sci., 16 **(2021)** Article ID: 210752, doi: 10.20964/2021.07.11

International Journal of
ELECTROCHEMICAL
SCIENCE
www.electrochemsci.org

Study of Novel Quinazolinone Derivatives with Different Chain Lengths as Corrosion Inhibitors for Copper in 0.5 M Sulfuric Acid Medium

Jian Zhang, Shengtao Zhang[*]

School of Chemistry and Chemical Engineering, Chongqing University, Chongqing 400044, China.
[*]E-mail: stzhangcqu@163.com

Received: 18 February 2021 / *Accepted:* 7 April 2021 / *Published:* 31 May 2021

Two new compounds based from quinazolinone derivatives namely, 6,7-dimethoxyethoxyquinazolin-4-one (DME) and 6,7-dimethoxyquinazolin-4-one (DM). By electrochemical measurements, their inhibitive ability in 0.5 M H_2SO_4 were studied for copper sample, It is seen that anti-corrosion performance is relative with solution concentration, the best value of corrosion inhibitive efficiency is 93.8%, 88.5% at 5 mM of DME and DM, respectively. The above results are also confirmed by surface analysis including SEM and AFM. The two quinazolinone derivatives adsorb on copper surface by Langmuir adsorption isotherm, and defined as physical adsorption. FT-IR and XPS results further confirm chemical bond between the studied molecules and Cu. The calculation results of quantum chemistry and molecular dynamics simulation further explain the reason that the parallel direction of DME with longer chain length can increase the contact area to the copper surface and better prevent the attack of corrosive media on copper.According to experimental and theoretical study, indicating that The longer the chain, the stronger the inhibitive ability,as DME >DM.

Keywords: Corrosion inhibitor, Quinazolinone derivatives, Surface analysis, FT-IR, Quantum chemistry

1. INTRODUCTION

Copper is used extensively in energy, chemical, electronics and other fields as the fifth wide usual metal. Copper and its alloys have the advantages of anti-corrosion ability, high electrical conductivity and thermal conductivity, excellent machinability and ductility. Although It will be corroded in an acidic environment, especially pitting corrosion on the copper surface, which will have a serious negative impact on the performance of the copper system and may reduce its use efficiency. In order to protect copper from corroding, adding corrosion inhibitors into corrosive medium has become a simple and feasible method. These organic molecules usually contain heteroatoms (such as O, N, P, S) and unsaturated bonds. The corrosion inhibition process includes two steps: the first step is to adsorb on the active site of the metal; the second step is to pass steric hindrance effect of organic molecules hinders the corrosive medium .[1-7].

At present, there are few literature reports about quinazolinone derivatives as corrosion inhibitors .To this end,we explore the inhibitive ability of two new quinazolinone derivatives with 6,7-dimethoxyethoxy-quinazolin-4-one(DME) and 6,7-dimethoxyquinazolin-4-one(DM). The electrochemical behavior of DME and DM is mainly studied by potential polarization curve (PDP) and electrochemical impedance spectroscopy (EIS). Surface morphology by scanning electron microscope (SEM) and atomic force microscope (AFM) will be evaluated. The calculation results of quantum chemistry and molecular dynamics simulation further illustrate interaction mechanism between compounds and Cu surface, and provide experience and reference for the design and development of new quinazolinone derivatives corrosion inhibitors.

2. EXPERIMENTAL

2.1 Electrode and material preparation

The Electrode in the all experiments was pure copper samples (99.6%).They were cut, polished and cleaned, and then enclosed in epoxy resin leaving 1cm^2 working area for electrochemical testing. The work electrode was rubbed continuously with 180#-2000# grit abrasive papers, then cleaned by ultrapure water (AFZ-1002-U, Taiwan Aikepu Water Treatment Company), alcohol and acetone,finally cold air drying.

The DME and DM were purchased from Shanghai Mindray Chemical Technology Co., Ltd. (manufacturer is Meryer) with the purity of 98.0%, and its structural formula are presented in Fig. 1.

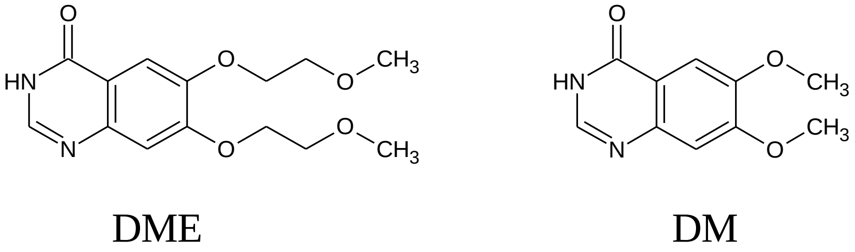

Figure 1. The molecular structures of DME and DM

Other reagents used in the experiment such as sulfuric acid (98%), acetone (99.5%) and ethanol (≥99.7%) were purchased from Chongqing Chuandong Chemical Group Co., Ltd.. The concentrated sulfuric acid (98%) was diluted to 0.5 mol/L H_2SO_4 solution (parallel group), then adding various doses(0.25, 0.5, 1, and 5 mM) into it. All experimental tests were kept at near 298 K by thermostat water bath (DK-96-II,Tianjin Test Instrument Co., Ltd.).

2.2 Electrochemical experiment

In order to get the relative electrochemical data of corrosion inhibition , the test including open circuit potential (OCP), EIS and PDP executed on the CHI760E electrochemical station (Shanghai Chenhua Co.,Ltd) was conducted in three-electrode system regarding copper , a saturated calomel electrode and a platinum foil (2 × 2× 0.2 cm) as working electrode, reference electrode and counter electrode.

First, for the sake of getting stable open circuit potential (E_{OCP}), the tesing system was kept for 1800 s. Then EIS was conducted at the base of $\mathrm{E_{OCP}}$ above. The signal amplitude was a 10 mV, the potential was E_{OCP}, the frequency was 100 kHz ~ 0.01 Hz. Finally, PDP were performed by a 2 mV s^{-1} scan rate,and polarization test of $\mathrm{E_{OCP}} \pm 250$ mV. The parallel test was 4 times.

2.3 Surface analysis

The SEM and AFM were employed to further study copper 2D and 3D surface topography,respectively. the chemical bond are reserched with the XPS and FT-IR. Before, the samples were soaked in a parallel group and 5 mM DME and DM test solution respectively , and soaking time is 36 h for SEM, 10 h for AFM and FT-IR, 16 h for XPS at 298 K.

2.4 Theoretical methods

The adsorption process between two quinazolinone derivatives and the Cu (111) surface was studied by theoretical methods including quantum chemical calculations with DMol3 module and molecular dynamics (MD) with NVT ensemble, 1000 ps simulation time,and 1.0 fs time step at 298 K. And then the optimized molecules structures and relative theoretical parameters were getted.

3. EXPERIMENTAL RESULTS AND ANALYSIS

3.1 Impedance spectrum experiments

For sake of knowing about anti-corrosion efficiency and kinetics process of two kinds molecules for Cu, the EIS for copper in a blank solution and a 0.5 M sulfuric acid solution containing four different doses of quinazolinone derivatives are conducted , Fig. 2 is the Nyqusit diagram.

In Figure. 2, the diagram of the blank group is composed of the high frequency semicircular capacitive loop related with the charge transfer resistance(R_{ct}) and the electric double layer capacitance(C_{dl}) and the low frequency Warburg straight line mainly due to the diffusion of copper ions and movement dissolved oxygen[2]. These semicircular arcs are all flattened, which is a unique phenomenon of solid electrodes. It shows that the Cu surface is rough and uneven. Compared with the parallel group, the capacitive arc radius visibly shows larger with the increase of the corrosion inhibitor content,which has a good anti-corrosion effect on copper[2,4]. When the highest 5 mM is reached, the Warburg impedance disappears, indicating that a dense protective film forms due to the two organic corrosion inhibitors DME and DM absorbed on the electrode surface, the diffusion process is strongly hindered, and the charge transfer plays a major process. Moreover, at different concentrations, the semicircular arc diameter of DME is significantly larger than that of DM, indicating that the corrosion inhibitor performance of DME is more than DM.

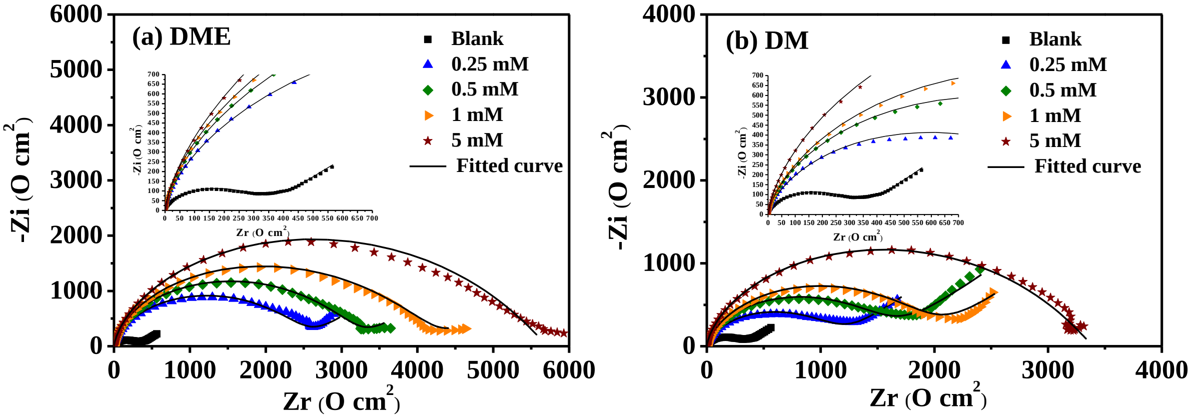

Figure 2. Nyqusit diagrams for copper in blank solution and diverse concentrations of (a) DME, (b) DM at 298 K.

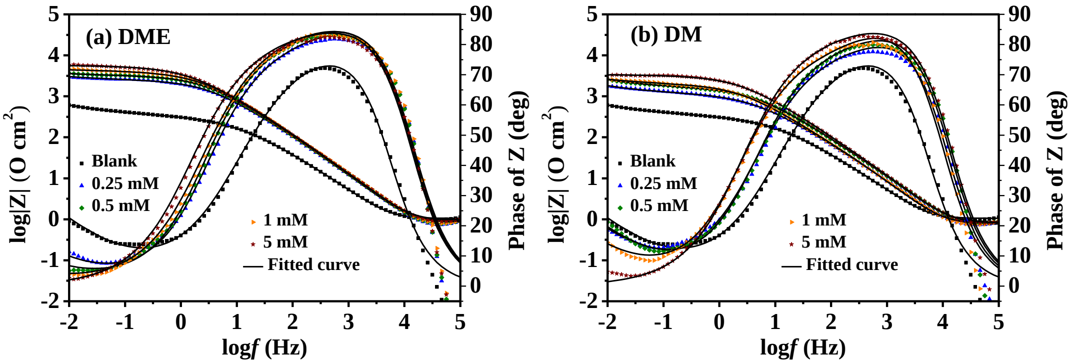

Figure 3. Bode plots present in **Figure 2**, (a) DME, (b)DM

Fig. 3 shows the Bode plots. As the corrosion inhibitor increases, impedance modulus value and maxmium phase angle range also gradually larger. In the intermediate frequency region, log|Z| and logf have a linear relationship with a slope of -1 , Which shows an obvious capacitive behavior, and DME and DM are uniformly adsorbed on the electrode surface [1]. In particular, the phase angle curve shows a time constant, which is caused by the relaxation effect of the electric double layer. All of that shown that both DME and DM can effectively suck on the copper surface, prohibiting the corrosion of copper , and the inhibitory effect of DME is greater than that of DM.

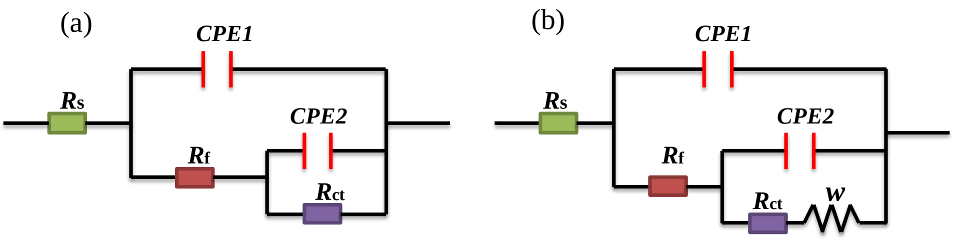

Figure 4. electrochemical equivalent circuitst fitted the impedance data.

For equivalent circuits in Fig. 4. Here, R_S presents the solution resistance, R_f is the film resistance, R_{ct}, *W*, *CPE*1 and *CPE*2 stand the charge transfer resistance, the Warburg impedance, film capacitance and double layer capacitance, respectively. Formula as follows [8-12]:

$$Z_{\text{CPE}} = \frac{1}{Y(j\omega)^n} \quad (1)$$

Among them, Y is the CPE constant, ω is the angular frequency, j is the imaginary root, and n presents the diffusion efect index. if n=1, CPE is a pure capacitor; if n=0.5, it stands Warburg impedance; if n=0, it is pure resistor. The C_{dl} value can be calculated by equation(2)[13-15]:

$$C_{\text{dl}} = Y(\omega)^{n-1} = Y(2\pi f_{Zim-Max})^{n-1} \quad (2)$$

The η of DME and DM was calculated by equation(3),respectively [16-20].

$$\eta = \frac{R_{\text{ct}} - R_{\text{ct,0}}}{R_{\text{ct}}} \times 100\% \quad (3)$$

In Table .1, when adding oriented molecules DME and DM, R_f and R_{ct} increase accordingly. It shows that both DME and DM can effectively form a protective film, thereby hindering charge transfer. In addition, as the concentration of inhibitors increases, the C_{dl} and C_f values are correspondingly reduced, which can be illustrated by the following parallel plate capacitance definition formula [21-23]:

$$C_{\text{dl}} = \frac{\varepsilon_0\, \varepsilon}{d} S \quad (4)$$

Here, d is the thickness of electric double layer, ε_0 and ε are the local dielectric constants of the air and the electric double layer, respectively, and S is the work area exposed to the solution.

When adding DME and DM, organic molecules gradually replace water molecules to occupy active sites, which will reduce ε, because the dielectric constant of organic matter is smaller than that of water [1,8]. At the same time, the volume of studied compounds is larger than water molecules, when the concentration increases, the thickness d of the electric double layer increases and the surface coverage increases, which makes the C_{dl} value less than that of the parallel group, and the C_{dl} of the DME is significantly lower than the DM. At the same time, n has always been between 0.5 and 1, which fully shows that the capacitance characteristic between the solution and the metal electrode is not a pure capacitance [9]. In the two kinds of sustained-release agents, with the addition of bisethoxy group, the electron donating effect is enhanced, and the ethoxy group-containing corrosion inhibitor molecule is more likely to give electrons to the empty orbital of the copper and then adsorb to the metal surface; The longer chains increases the coverage of the DME, protecting copper from the aggressive medium validly and then shows a better corrosion inhibition effect.As a result, inhibition efficiencies reach 93.8% for DME, 88.5% for DM.

Therefore, the addition of bisethoxy group increases the chain length and active sites, and significantly increases the performance of the corrosion inhibitor.

Table 1. Impedance parameters for copper in blank solution and various concentrations of corrosion inhabitor at 298 K.

C (mmol/L)	R_s (Ω cm^2)	R_f (Ω cm^2)	R_{ct} (Ω cm^2)	R_p (Ω cm^2)	C_f (μF cm^{-2})	Y_0 (μ Ω^{-1} s^n cm^{-2})	n_2	C_{dl} (μF cm^{-2})	W (*10-2)	η (%)
Blank	1.51	11.97	344.2	356.2	28.44	29.54	0.57	6.4	1.21	—
DME										
0.25	0.85	169.0	2384	2553.0	13.14	49.04	0.64	17.7	0.59	86.0
0.5	0.88	212.8	3070	3282.8	12.69	43.15	0.61	15.6	0.80	89.2
1	0.88	150.8	4201	4351.8	11.88	45.54	0.57	16.0	1.49	91.8
5	0.96	138.2	5578	5716.2	12.16	39.39	0.60	17.5	—	93.8
DM										
0.25	0.77	36.53	1159	1195.5	17.60	101.5	0.62	35.4	0.49	70.2
0.5	0.86	80.38	1566	1646.4	13.87	63.88	0.63	24.2	0.34	78.4
1	0.81	116.6	1899	2015.6	18.96	73.28	0.65	31.4	0.48	82.3
5	0.83	126.8	3269	3395.8	13.32	48.73	0.59	18.3	—	88.5

3.2 Potentiodynamic polarization curve

Fig. 5 is the PDP plots, It shows that the blank polarization curve has the highest current density, when increasing corrosion inhibitors, corrosion current density is gradually reduced and Tafel curve moves negatively, and the reduction of the current density is reflected in both the cathode branch and the anode branch [11,12].

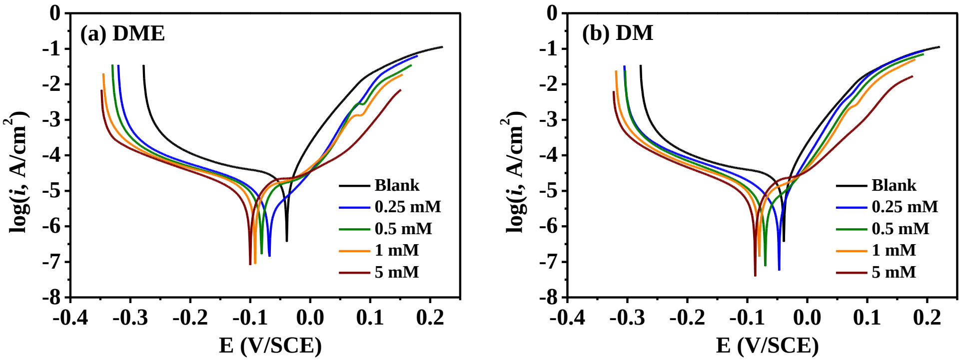

Figure 5. Potentiodynamic polarization curves for copper in blank solution and diverse concentrations of (a) DME, (b) DM at 298 K.

Table 2. Potentiodynamic polarization parameters for copper in blank solution and diverse concentrations of DME and DM at 298 K.

T (K)	C (mmol/L)	$-E_{corr}$ (V/SCE)	i_{corr} (μAcm^{-2})	$-\beta_c$ (mV dec^{-1})	β_a (mVdec^{-1})	η (%)
Blank	0.00	0.039	41.10	379	59	-
DME	0.25	0.068	6.510	193	61	84.2
	0.5	0.082	6.173	74	41	85.0
	1	0.091	6.027	40	62	85.3
	5	0.101	4.874	46	60	88.1
DM	0.25	0.047	9.216	174	70	77.6
	0.5	0.069	9.062	120	57	78.0
	1	0.079	6.946	52	62	83.1
	5	0.087	5.762	85	48	86.0

The relative data of Table 2 is getted by extrapolation, including the corrosion current density (i_{corr}), corrosion potential (E_{corr}), Tafel slope of cathode and anode (β_c, β_a). η was calculated by the Equation (5), [24-28]:

$$\eta = \left(\frac{i_{corr,0} - i_{corr}}{i_{corr,0}}\right) \times 100\% \qquad (5)$$

where $i_{corr,0}$ and i_{corr} shows corrosion current density with unprotected and protected the copper samples,respectively.

The data in Table 2 shows that the shifting of E_{corr} is less than 85 mV, the results reveal that DME and DM are considered to be a mixed type inhibitor, which not only inhibits the reaction of the anode but also the reaction of the cathode [21,24]. As the concentration of inhibitors increases, E_{corr} gradually shifts negatively, i_{corr} gradually decreases, and η gradually increases. When the concentration of the two corrosion inhibitors is 5 mM, the current density decreases most obviously, and the anti-corrosion efficiency is the best, which are 88.0% for DME and 86.0% for DM, respectively. At the same time, it can be seen that the inhibitory effect of DME is greater than that of DM, that is consistent with electrochemical impedance spectroscopy data above.

Therefore, the two kinds quinazolinone derivatives are effective inhibitors, and DME with longer bisethoxy group chain length has a better protective ability on copper.

3.3 Scanning electron microscopy analysis

In order to analyze the 2D morphology of the copper electrode immersed in blank solution and 5 mM inhibitors at 298 K. In Figure 3.6(a), the fresh copper surface is clean and even, and only some traces of sandpaper polishing are seen. However, the copper surface immersed in blank solution was severely corroded, and the surface was rough and uneven. Figure 3.6(c,d) shows that the copper surface after adding DME and DM is well protected and the surface is relatively smooth.

By comparing the two corrosion inhibitors of DME and DM, the degree of the surface roughness: DM > DME, it reflects the protective ability of the corrosion inhibitor to copper. Therfore, the protective effect of DME owing longer chain is stronger than that of DM. This verificates directly the electrochemical analysis above.

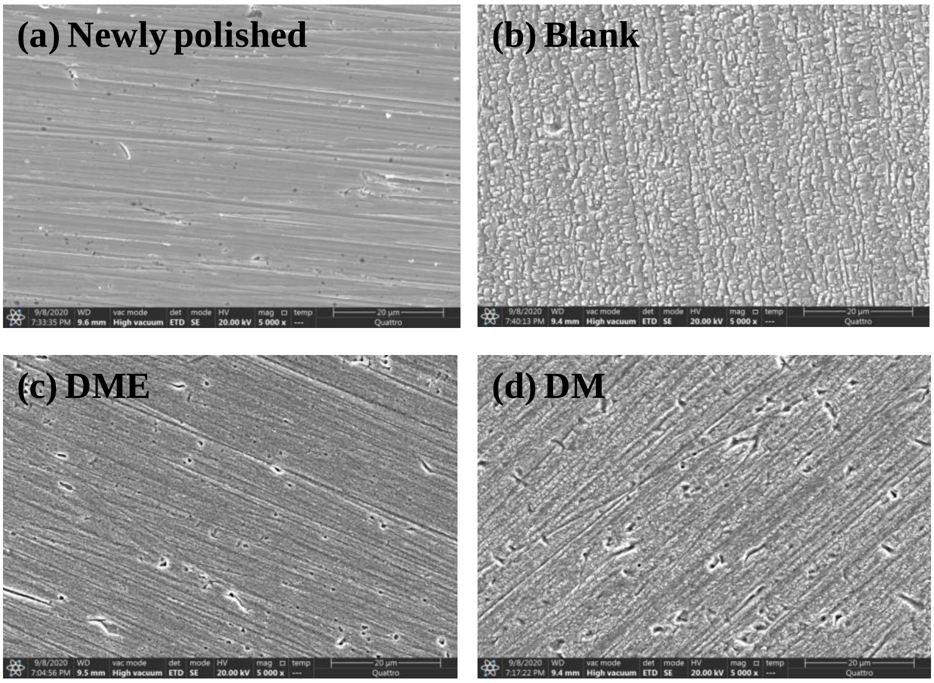

Figure 6. SEM 2D morphologies of the copper specimen soaked in blank solution and with 5 mM inhibitors at 298 K for 36 h, newly polished (a); blank solution (b); DME (c); DM(d)

3.4 Atomic force microscopy analysis

AFM 3D pictures and height profiles of newly polished (a, b), unprotected copper (c, d), protected copper by DME (e, f) and DM (g, h) are shown in Fig. 7.

Figure 3.7(a) is a freshly polished copper sample, It can be seen that the surface is very smooth and flat. Figure 3.7(c) is a 3D image after soaking in the blank solution. The surface is corroded severely and has deep groove marks. Compared with Figure 3.7(e) and (f), it is clear that with the addition of DME and DM, its surface becomes relatively smooth and flat. In addition, since the average roughness represents the corrosion inhibition ability, the smaller the average roughness, the stronger the corrosion inhibition performance. The average roughness (R_a) of the blank solution was 41.5 nm, but after adding DME and DM, its Ra was reduced to 20.9 nm and 22.6 nm, respectively. Therefore, the two quinazolinone derivatives studied have a better protective effect for copper, but the anti-corrosion ability of DME is stronger than DM. This may be due to the different molecular chain lengths of the two corrosion inhibitors. The longer chain length has a better corrosive inbitive effect.This is consistent with the conclusions drawn by electrochemical data analysis and scanning electron microscopy analysis.

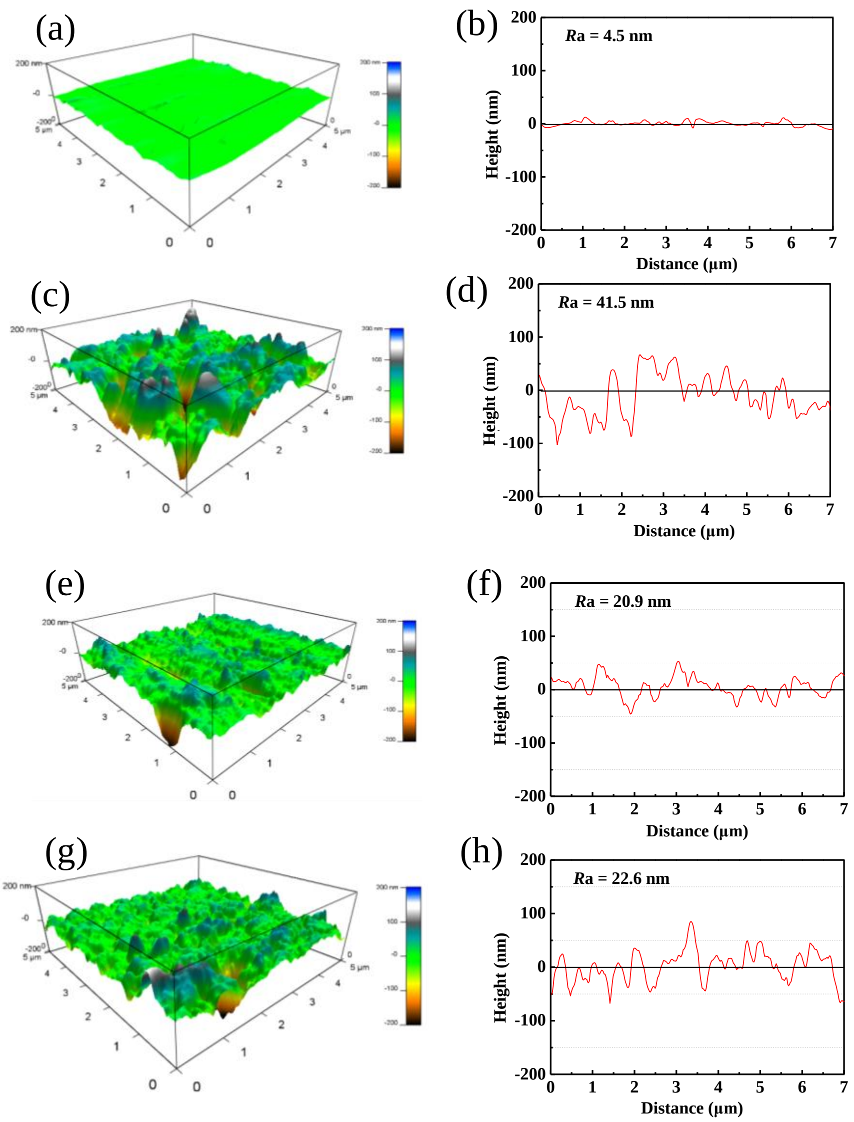

Figure 7. AFM 3D and height profile images of newly polished (a, b), unprotected copper (c, d), protected copper by DME (e, f) and DM (g, h) for soaking10 h at 298 K.

3.5 FT-IR analysis

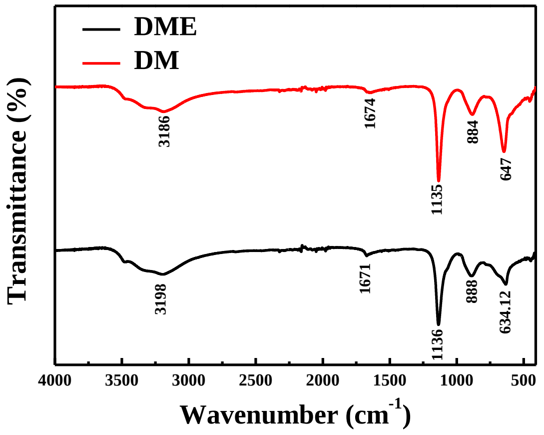

Figure 8. FTIR spectrum of DME and DM.

FT-IR image is presented in Fig. 8 including DM and DME. The broad peak at around 3186 cm^{-1} and 3198 cm^{-1} is related to the contamination of H_2O and the vibration of C-H bonds from phenyl groups. The variation of C=O,C=N and C=C symmetric stretching vibration peak is observed at 1674 cm^{-1} and 1671 cm^{-1} .The variation of C-O-C is observed at 1135 cm^{-1} and 1136 cm^{-1}. All group above of which verify that the DME and DM can adsorb copper surface effectively.

3.6 XPS analysis

The XPS were carried out to analyze interaction between copper and two kinds oriented compound DME and DM. In Fig. 9, the C, Cu, N and O elements can be detected in Cu-DME, Cu-DM, all fitting data are shown in Table 3.In Fig. 9(a,e) , characteristic spectra of C1s includes C-O/C=O,C-N, C=N, and C-C, corresponding peak position is 288.37 eV, 286.36 eV, 285.10 eV, 284.80 eV for DME and 288.00 eV,286.37 eV,285.25 eV, 284.62 eV for DM. In Fig. 9(b,f), for Cu2p , the peaks at about 952.50 eV, 932.70 eV for DME and 951.45 eV,932.10 eV for DM are atributed to Cu 2p 1/2 and Cu(0)/Cu(I)，respectively.but the peak of Cu(Ⅱ) is not found. Fig. 9(c,g) for N1s , the peaks at about 400.35 eV, 399.44 eV, 399.16 eV for DME and 399.30 eV,398.78 eV , 398.50 eV for DM are relative with N-Cu, N-C and N=C. The N-Cu bond is origined from the chemical reaction of nitrogen and copper ions. Fig. 9(d,h) shows the characteristic peaks of O1s containing CuO/Cu_2O , C-O and C=O , the position is 532.60 eV,531.69 eV ,530.72 eV for DME and 531.99 eV,531.06 eV,530.10 eV for DM.

These group suggest that DME and DM can adsorb on the Cu surface, then inhibit copper surfaces to be corroded further.

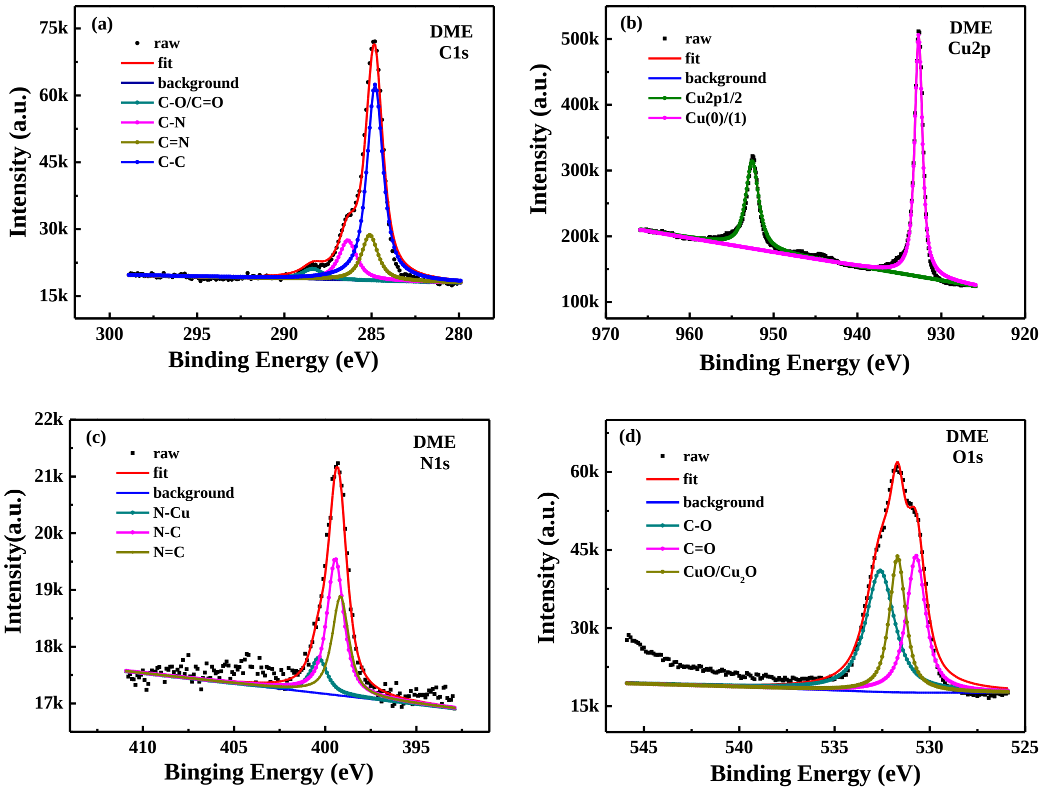

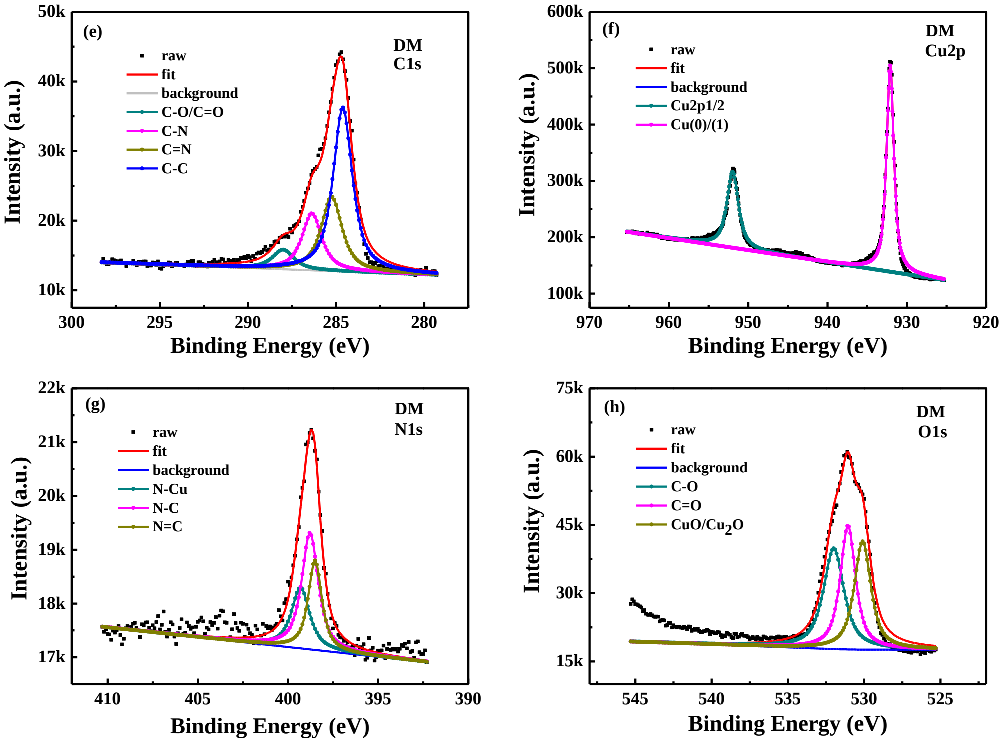

Figure 9. XPS spectra for DME and DM

Table 3. The fitting XPS spectra parameter of DME and DM

Level	Sample	State	E_B	FWHM
Cu2p	Cu-DME	Cu2p1/2	952.50	1.10
		Cu(O)/(I)	932.70	1.10
	Cu-DM	Cu2p1/2	951.45	1.74
		Cu(O)/(I)	932.10	1.10
C1s	C-DME	C-O/C=O	288.37	1.44
		C-N	286.36	1.22
		C=N	285.10	1.13
		C-C	284.80	1.10
	C-DM	C-O/C=O	288.00	1.45
		C-N	286.37	1.33
		C=N	285.25	1.40
		C-C	284.62	1.30
N1s	N-DME	N-Cu	400.35	1.10
		N-C	399.44	1.10
		N=C	399.16	1.10
	N-DM	N-Cu	399.30	1.20
		N-C	398.78	1.10
		N=C	398.50	0.90
O1s	O-DME	C-O	532.60	1.80
		C=O	531.69	1.01
		CuO/ Cu_2O	530.72	1.20
	O-DM	C-O	531.99	1.60
		C=O	531.06	1.20
		CuO/ Cu_2O	530.10	1.30

3.7 Adsorption isotherm studies

For sake of further exploring adsorption mechanism of inhibitors in the interface, the electrochemical impedance measurement results are used to fitting. The fitting formula is shown in Equation (6) [29-32]. The fitting results show that R^2 is close to 1 at 298 K, the adsorption process of DME and DM meets the Langmuir adsorption isotherm. The related fitting line and thermodynamic parameters are shown in Fig. 10.

$$\frac{C}{\theta}=\frac{1}{K_{ads}}+c \qquad (6)$$

where θ is the surface coverage from EIS data, K_{ads} is the equilibrium constant of the adsorption process, and C is the inhibitors concentration.

ΔG_{ads}^{0} refers the formula (7):

$$\mathrm{K_{ads}}=\frac{1}{55.5}\exp\left(\frac{-\Delta \mathrm{G}_{\mathrm{ads}}^{0}}{\mathrm{RT}}\right) \qquad (7)$$

Here, R is the universal gas constant; T is the absolute temperature.

Generally speaking, the smaller ΔG_{ads}^{0} and the larger K_{ads} indicate that studied inhibitors are more likely adsorbed on the metal surface, thus having better corrosion inhibition performance [33-35]. As shown in Fig. 10, after adding two molecules DME and DM: the order of K_{ads} is: DME > DM; $\Delta G_{ads}^{0}$is a negative value, and its values are -18.80 kJ/mol for DME and -16.02 kJ/ mol for DM, that is, DME <DM. The above data indicates that two quinazolinone derivatives molecules with different chain lengths on the copper surface is a spontaneous adsorption process, and the longer chain length DME has better adsorption capacity and is adsorbed to the electrode surface by physical adsorption[36].

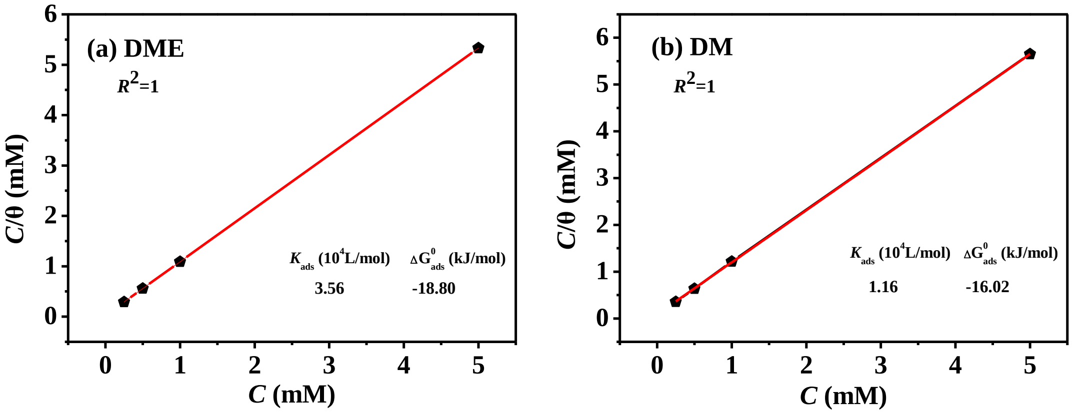

Figure10. Langmuir adsorption isotherms and corresponding thermodynamic parameters of two molecules, (a)DME, (b) DM.

3.8 Quantum Chemistry Study

The quantum chemical calculations were performed to know interaction means of target DME and DM on the copper.The Fig. 11 shows corresponding molecular optimized structure, the highest occupied molecular oribital (HOMO) and the lowest empty molecular oribital (LUMO) for DME and DM. It can be seen that the acitive site of DME and DM are mainly concentrated on the quinazolinone ring, including O, N, double bond and benzene ring, and slightly distributed on the substituent methoxy group. It shows that the quinazolinone ring is the main active center of adsorption.

As we all know, the higher E_{HOMO} reflects the stronger electron-devoting, while lower E_{LUMO} indicates that molecules tend to accept electrons [1, 29, 33-36]. The smaller value of ΔE reflects , the stronger adsorption ability on the copper is[37], and then obtaining a higher anti-corrosion efficiency. It can be seen from Table 4 that DME has a smaller energy gap value, and has higher reactivity than DM. The results above are consistent with anti-corrosion ability. The long chain length of corrosion inhibitor molecules will produce a larger coverage area, increase steric hindrance, and protect copper from corroding.

In addition, the dipole moment (μ) value of 2.220 Debye for DME also has a lower than 3.910 Debye of DM. According to literature reports, in general, molecules with larger μ represent stronger corrosion inhibition efficiency [1,16,24]. However, the value of μ and anti-corrosion efficiency here does not completely correspond. It can be understood that the dipole moment is a vector with both magnitude and direction [38]. It is the product of the distance between the centers of positive and negative charges and the amount of charge. Due to the different molecules structure, the direction of the dipole moment, the charge, etc. is different, so here we cannot simply judge the corrosion inhibition efficiency based on the value of the dipole moment.

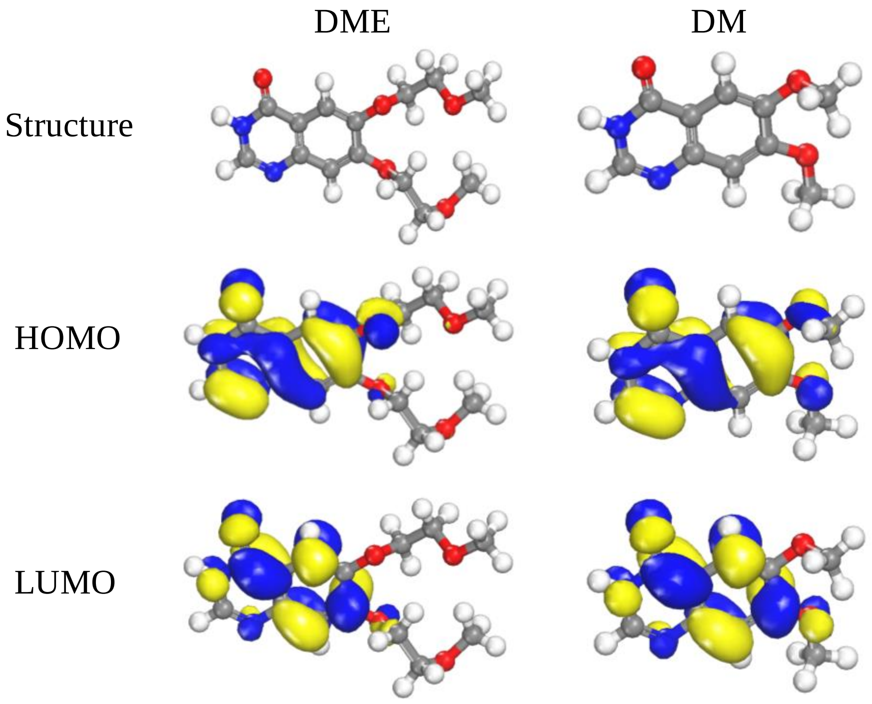

Figure 11. the optimized structures,HOMO and LUMO for studied DME and DM.

Table 4. The relative theoretical calculation parameters for DME and DM.

Species	E_{HOMO} (eV)	E_{LUMO} (eV)	ΔE (eV)	μ(D)
DME	-5.754	-1.978	3.776	2.220
DM	-5.704	-1.857	3.847	3.910

3.9 MD RESEARCH

MD can be used to study the interaction between oriented molecules and copper surface. The equilibrium adsorption model of two quinazolinone derivatives with different chain lengths on the copper surface and relevant paremeters were presented in Fig. 12 and Table 5,respectively. The side view observes that the DME and DM are adsorbed in parallel on the Cu(111) surface. From the top view, it can be seen that the longer chain length DME molecule can increase the contact area and better prevent the attack of corrosive medium. In addition, the interaction energy($E_{interact}$) and binding energy y ($E_{binding}$) can be calculated by formulas (8,9)[39-41]:

$$E_{interact} = E_{tot} - E_{inh} - E_{subs} \tag{8}$$

$$E_{bingding} = -E_{interact} \tag{9}$$

Here, E_{tot} ,E_{subs} and E_{inh} present the sum of the system energies, the copper substrate energy of H_2O molecules and the energy of inhibitor, respectively.

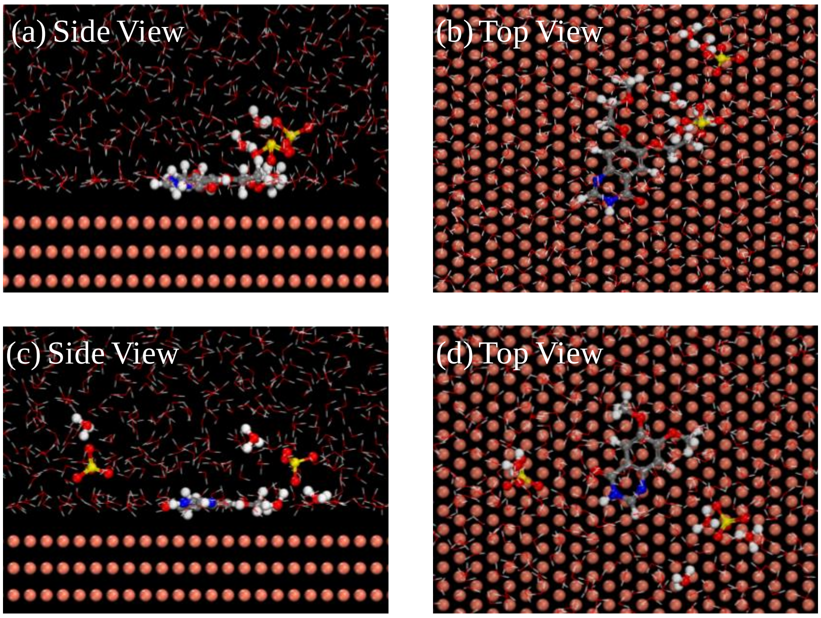

Figure 12. Equilibrium adsorption configurations (side and top view) of two investigated inhibitors on Cu (111) substrate, (a,b) DME, (c,f) DM.

Generally speaking, the larger the E_{binding}, the tighter the corrosion inhibitor molecules absorbed on metal surface are, and the higher anti-corrosion efficiency is. The computered value of $E_{binding}$ are 210.3 kJ/mol for DME and 108.7 kJ/mol for DM,It is clear that E_{binding} of DME is significantly greater than DM. This result verifys the data obtained from electrochemical experiments and the results of the characterization data, verifying that DME molecules with longer chain lengths have better corrosion inhibition efficiency.

In particular, the RDF obtained from MD simulation is an effective parameter reflecting the characteristics of chemical bonds. It is worth noting that the peak position less than 3.5 Å represents chemical adsorption, and the peak position greater than 3.5 Å represents physical adsorption. As shown in Figure. 13, the bond lengths of the heterocyclic N atoms and O atoms in the DME with Cu are greater than 3.5 Å, indicating the excellent inhibitory properties of the studies compounds.

Table 5. The relevant parameters of the molecular dynamics simulation of DME, DM on the copper surface

	E_{total} (kJ mol^{-1})	$E_{\mathrm{inhibitor}}$ (kJ mol^{-1})	E_{sub} (kJ mol^{-1})	E_{binding}(kJ mol^{-1})
DME	-4735.7	-39.5	-4645.9	210.3
DM	-4845.8	-31.8	-4788.0	108.7

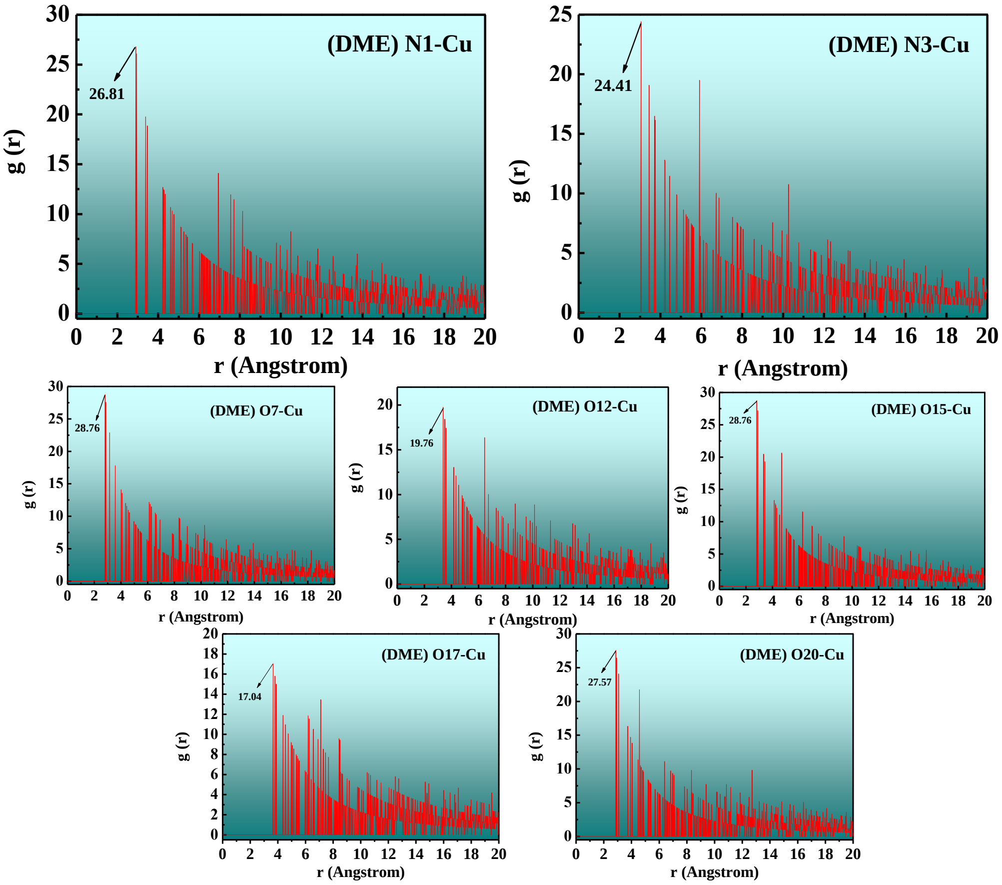

Figure 1. The RDF of DME molecules on Cu (111).

4. CONCLUSIONS

Two new quinazolinone derivatives from namely, 6,7-dimethoxyethoxy-quinazolin-4-one (DME) and 6,7-dimethoxyquinazolin-4-one (DM) were prepared. Then, inhibition efficiency of DME and DM for copper in 0.5 M H_2SO_4 solution was researched by using electrochemical methods,surface analysis and instrument characterization and theory calculation. The conclusions are getted by the studies above:

(1) The electrochemical results show that the two kinds of molecules with different chain lengths can inhibit copper corrosion, but the longer chain length DME has higher corrosion inhibition efficiency. The Tafel curve shows that the two corrosion inhibitors are mixed type inhibitor suppressing mainly the cathode.

(2) The reliability of electrochemical data was verified by SEM and AFM surface analysis.

(3) The adsorption process of the two molecules obeys the Langmuir adsorption model, and acts on the copper surface through physical adsorption.

(4) The theoretical results further explain: DME molecule with longer chain lengths owns stronger adsorption ability, maximizes the contact area with the copper surface, effectively inhibits the contact of the corrosive medium, and then achieving higher corrosion inhibition performance.

ACKNOWLEDGMENTS
This work was supported financially by National Natural Science Foundation of China (No. 21878029, and 21676035), the Sail plan of Guangdong, China (No. 2015YT02D025).

References

1. B. Tan, J. He, S. Zhang, C. Xu, S. Chen, H. Liu, and W. Li, *J. Colloid Interf. Sci*., 585 (2021) 287.
2. X. Zuo, W. Li, W. Luo, X. Zhang, Y. Qiang, J. Zhang, H. Li, and B. Tan, *J. Mol. Liq*., 321 (2021) 114914.
3. L.O. Olasunkanmi, and E.E. Ebenso, *J. Colloid Interf. Sci.*, 561 (2020) 104.
4. L. Guo, J. Tan, S. Kaya, S. Leng, Q. Li, and F. Zhang, *J. Colloid Interf. Sci.*, 570 (2020) 116.
5. J. Tang, Y. Hu, H. Wang, Y. Zhu, Y. Wang, Z. Nie, Y. Wang, and B. Normand, *Int. J. Electrochem. Sci.*, 14 (2019) 2246.
6. A. S. Fouda, M. Abdel Azeem, S.A. Mohamed, A. El-Hossiany, and E. El-Desouky, *Int. J. Electrochem. Sci.*, 14 (2019) 3932-3948.
7. I. Martinović, G.Z. Zora Pilić, L. Šušić, O. Kowalska, D. Petrović, F. Falak, and J. Mišković, *Int. J. Electrochem. Sci.*, 14 (2019) 4206.
8. B. Tan, S. Zhang, Y. Qiang, W. Li, H. Li, L. Feng, L. Guo, C. Xu, S. Chen, and G. Zhang, *J. Mol. Liq*., 298 (2020) 111975.
9. A. Singh, K.R. Ansari, D.S. Chauhan, M.A. Quraishi, H. Lgaz, and I.M. Chung, *J. Colloid Interf. Sci.*, 560 (2020) 225.
10. Y.J. Yang, Y. Li, L. Wang, H. Liu, D.M. Lu, and L. Peng, *Int. J. Electrochem. Sci.*, 14 (2019) 3375.
11. S. Xu, W. Li, X. Zuo, D. Zheng, X. Zheng, and S. Zhang, *Int. J. Electrochem. Sci*., 14 (2019) 5777.
12. S. Tao, and H. Huang, *Int. J. Electrochem. Sci.*, 14 (2019) 5435-5447.
13. B. Tan, B. Xiang, S. Zhang, Y. Qiang, L. Xu, S. Chen, and J. He, *J Colloid Interf. Sci.*, 582 (2020) 918-931.

14. J. Liu, Y. Zhou, C. Zhou, and H. Lu, *Int. J. Electrochem. Sci.*, 15 (2020) 2499.
15. N. V. Likhanova, P. Arellanes-Lozada, O. Olivares-Xometl, I.V. Lijanova, J. Arriola-Morales, J.C. Mendoza-Hérnandez, and G. Corro, *Int. J. Electrochem. Sci.*, 14 (2019) 2655-2671.
16. B. Tan, S. Zhang, Y. Qiang, W. Li, H. Liu, C. Xu, and S. Chen, *J. Mol. Liq.*, 286 (2019) 110891.
17. Q.H. Zhang, B.S. Hou, and G.A. Zhang, *J. Colloid Interf. Sci*., 572 (2020) 91.
18. K.R. Ansari, D.S. Chauhan, M.A. Quraishi, and T.A. Saleh, *J Colloid Interf. Sci*., 564 (2020) 124.
19. J. Zhang, *Int. J. Electrochem. Sci.*, 15 (2020) 1437.
20. C. Wang, W. Gou, C. Liu, D. Fu, L. Zhou, C. Lai, B. Xie, and S. Zhu, *Int. J. Electrochem. Sci.*, 14 (2019) 3443.
21. B. Tan, S. Zhang, H. Liu, Y. Qiang, W. Li, L. Guo, and S. Chen, *J. Taiwan Inst. Chem. E.*,102 (2019) 424.
22. F. Bahremand, T. Shahrabi, and B. Ramezanzadeh, *J. Colloid Interf. Sci*., 582 (2021) 342.
23. S. Y. Al-Nami, *Int. J. Electrochem. Sci.*, 14 (2019) 3986.
24. B. Tan, S. Zhang, H. Liu, Y. Guo, Y. Qiang, W. Li, L. Guo, C. Xu, and S. Chen, *J. Colloid Interf. Sci*., 538 (2019) 519.
25. S. Chen, S. Chen, B. Zhu, C. Huang, and W. Li, *J. Mol. Liq.*, 311 (2020) 113312.
26. X. Ren, S. Xu, X. Gu, B. Tan, J. Hao, L. Feng, W. Ren, F. Gao, S. Zhang, Y. Xiao, and L. Huang, *J Colloid Interf. Sci.*, 585 (2021) 614.
27. Z. Xiao, Z. Zhou, L. Song, D. Wu, C. Zeng, and Z. Cao, *Int. J. Electrochem. Sci*., 14 (2019) 4705-4717.
28. X. Wang, H. Jiang, D. Zhang, L. Hou, and W. Zhou, *Int. J. Electrochem. Sci.*, 14 (2019) 1178.
29. B. Tan, S. Zhang, W. Li, X. Zuo, Y. Qiang, L. Xu, J. Hao, and S. Chen, *J. Ind. Eng. Chem.*, 77 (2019) 449.
30. Y. Qiang, L. Guo, H. Li, and X. Lan, *Chem. Eng. J.*, 406 (2021) 126863.
31. Y. Qiang, S. Zhang, H. Zhao, B. Tan, and L. Wang, *Corros. Sci.*,161 (2019) 108193.
32. S. Chen, H. Zhao, S. Chen, P. Wen, H. Wang, and W. Li, *J. Mol. Liq.*, 312 (2020) 113433.
33. B. Tan, S. Zhang, Y. Qiang, L. Guo, L. Feng, C. Liao, Y. Xu, and S. Chen, *J. Colloid Interf. Sci.*, 526 (2018) 268.
34. Y. Qiang, H. Li, and X. Lan, *J. Mater. Sci. Technol.*, 52 (2020) 63.
35. L. Guo, B. Tan, X. Zuo, W. Li, S. Leng, and X. Zheng, *J. Mol. Liq.*, 317 (2020) 113915.
36. B. Tan, S. Zhang, Y. Qiang, L. Feng, C. Liao, Y. Xu, and S. Chen, *J. Mol. Liq*., 248 (2017) 902.
37. J. He, D. Yu, Q. Xu, G. Li, G. Chen, J. An, J. Yang, and W. Li, *J. Mol. Liq.*, 325 (2021) 115145.
38. M. Tabatabaei majd, S. Akbarzadeh, M. Ramezanzadeh, G. Bahlakeh, and B. Ramezanzadeh, *J. Mol. Liq.*, 297 (2020) 111862.
39. W. Luo, W. Li, J. Tan, J. Liu, B. Tan, X. Zuo, Z. Wang, and X. Zhang, *J. Mol. Liq.*, 314 (2020) 113630.
40. L. Guo, R. Zhang, B. Tan, W. Li, H. Liu, and S. Wu, *J. Mol. Liq.*, 310 (2020) 113239
41. X. Zhang, W. Li, X. Zuo, B. Tan, C. Xu, and S. Zhang, *J. Mol. Liq.*, 325 (2021) 115214